Pore Structure of Modified Cyclic Silsesquioxane Thin Films Made Porous Using a Cyclodextrins-Based Porogen

Jin-Heong Yim,*,† Mikhail R. Baklanov,‡ David W. Gidley,§ Huagen Peng,|| Hyun-Dam Jeong,† and Lyong Sun Pu†,⊥

Electronic Materials Lab., Samsung Advanced Institute of Technology (SAIT), San 14-1, Nongseo-ri, Kiheung-eup, Yongin-shi, Kyungki-do, 449-712, Korea, IMEC, Kapeldreef 75, B-3001 Leuven, Belgium, Department of Physics and Department of Materials Science and Engineering, University of Michigan, Ann Arbor, Michigan 48109, and Department of Advanced Materials, Sungkyunkwan University, 300 Chunchun-Dong, Jangan-Gu, Suwon, Kyungki-do, Korea, 440-746

Received: January 19, 2004

The pore structure of porous modified cyclic silsesquioxane (mCSSQ) thin films with different porogen concentration were investigated by means of EP and PALS as a "round robin" experiment. A plausible pore structure and its evolution as a function of porogen concentration (and hence porosity) can be deduced. At low concentration the cyclodextrin-based porogen molecules may be singly dispersed, resulting in isolated pores, while porogen agglomeration and pore collapse become severe with increasing concentration. The porosity increases and pore size distribution become broad with increasing porogen concentration. An interconnected cylinder-like pore shape can be postulated on the basis of the tendency for CD molecules to linearly interact. The dielectric constant and mechanical property of the porous mCSSQ thin films are strongly affected by the film's porosity.

1. Introduction

Porous materials have been researched extensively for many applications such as catalysts, adsorbents, membranes, sensors, and waveguides.[1−6] In particular, many porous thin films have been demonstrated as low-*k* (low dielectric) materials in large-scale integrated circuits (LSI) to reduce RC (resistance and capacitance) delay. One approach to generating nanoporous structures in thin films is to formulate a thermally stable low-*k* precursor with a pore generator (porogen) that can be decomposed and volatilized at the high temperature to leave pores in the film. The pore structure can be controlled by using different types of porogen. Typical examples of porogen are polymeric materials such as hyperbranched/star-shaped poly(caprolactone)[7,8] and poly(norbornene)[9] or ionic as well as nonionic surfactant such as CTAB (cetyltrimethylammonium bromide)[10] and poly(ethylene oxide-*b*-propylene oxide-*b*-ethylene oxide).[10,11] Recently, we have introduced the potential of making porous thin films with cyclodextrin (CD) as the pore-generating material.[12] The CDs are cyclic oligosaccharides consisting of at least six glucopyranose units that are joined together by α-(1→4) linkages. The CD compounds have three-dimensional structure with maximum diameter varying from 13.7 to 16.9 Å. These CDs could be molecularly dispersed in the film, acting like a single nanoparticle in the matrix precursor and making *isolated* nanopore via their decomposition. A study of the variation of porous structure for the thin films as a function of the CD porogen concentration has not been extensively explored in previous work.

It is important to understand pore structure such as pore size, shape, distribution, and total porosity in order to design a reliable low-*k* interlayer dielectric in an LSI device. For example, porosity must be high enough to ensure a low dielectric constant, *k*; pore size should be sufficiently smaller than the minimum feature size of the device; and the pore size distribution should be narrow enough to avoid film nonuniformity and poor process controllability. In characterizing pore structure we will follow the recommendations for characterization of nanopores as given by the International Union for Pure and Applied Chemistry (IUPAC).[13] According to the IUPAC definition, micropores have diameters smaller than 2 nm, while mesopores have diameters between 2 and 50 nm. Techniques for probing pore structure include nondestructive methods such as ellipsometric porosimetry (EP),[14] positronium annihilation lifetime spectroscopy (PALS),[15] and small angle neutron and X-ray scattering spectroscopy (SANS and SAXS) combined with specular X-ray reflectivity (SXR).[16−17] In this study, we use EP and PALS to investigate the pore structure of modified cyclic silsesquioxane (mCSSQ) thin films made porous by decomposition of varying concentrations of CD porogen. For systematic comparison, porous films cut from the same wafer are divided into pieces and subjected to characterization by the different technique. The evolution of the pore structure to that of a porous network with increasing porogen concentration is deduced from the EP and PALS results. In addition, the dielectric constant and mechanical properties of porous mCSSQ thin films having different pore structure were also monitored.

2. Experimental Section

2.1. Materials. Methyl trimethoxysilane and 2,4,6,8-tetramethyl-2,4,6,8-tetravinylcyclotetrasiloxane (Aldrich Chemical

* To whom correspondence should be addressed. Tel: 82-31-280-6732. Fax: 82-31-280-6725. E-mail: ch20889@sait.samsung.co.kr.
† Samsung Advanced Institute of Technology.
‡ IMEC.
§ Department of Physics, University of Michigan.
|| Department of Materials Science and Engineering, University of Michigan.
⊥ Sungkyunkwan University.

10.1021/jp049738j CCC: $27.50
Published on Web 06/03/2004

Co.) were used as received. Catalysts such as hydrochloric acid (Samchun Pure Chemical Co., Ltd) and platinum (*O*)-1,3-divinyl-1,1,3,3-tetramethyldisiloxane complex in xylene (Aldrich Chemical Co.) were also used as received. Triethylamine (Aldrich Chemical Co.), anhydrous sodium sulfate (Samchun Pure Chemical Co., LTD), methyl alcohol (Aldrich Chemical Co.), and 4-methyl-2-pentanone (Aldrich Chemical Co.) were used as received without further purification. Heptakis(2,3,6-tri-*O*-methyl)-β-cyclodextrin (CYCLO LAB. Co.) was used as received. Solvents such as tetrahydrofuran (J. T. Baker), diethyl ether (J. T. Baker), and acetone (J. T. Baker) were purified by distillation in the presence of sodium under N_2 atmosphere.

2.2. Synthesis of Modified Cyclic Silsesquioxane (mCSSQ) Precursors. In this study, MTMS (methyltrimethoxysilane) and TCS (2,4,6,8-tetramethyl-2,4,6,8-tetrakis(trimethoxysilylethyl)-cyclotetrasiloxane) were used as monomers to synthesize the matrix precursor. The mCSSQ precursor was prepared by acid-catalyst-controlled hydrolytic polycondensation of methyltrimethoxysilane and 2,4,6,8-tetramethyl-2,4,6,8-tetrakis(trimethoxysilylethyl)cyclotetrasiloxane.[18] The Si−OH content of the mCSSQ precursor, calculated by ^{1}H NMR (Bruker AM300), was 30.2 mol %, and the weight-average molecular weight (M_w) and polydispersity, measured by gel permeation chromatography (Waters 2690), were 4194 and 1.82, respectively.

2.3. Preparation of Porous Thin Films. The spin-on coating solutions were prepared by properly mixing the mCSSQ precursor as a matrix with heptakis(2,3,6-tri-*O*-methyl)-β-cyclodextrin (tCD) as a porogen and propylene glycol methyl ether acetate (PGMEA) as a solvent. The solution was spin-cast for 30 s at 3000 rpm, onto silicon wafers. The wafers were then subjected to a series of soft baking on a hot plate, including 1 min at 150 °C and another minute at 250 °C to remove the organic solvent. The porous thin films were then produced by curing the wafers in a cylindrical furnace (Linberg type 55642) at 420 °C for 60 min under vacuum.

2.4. Characterization of Porous Thin Films. The film porosity and pore radius distribution (PRD) were analyzed by ellipsometric porosimetry.[14] Ellipsometric porosimetry is a combination of nonintrusive (wave propagation) and intrusive (adsorption) methods. Full porosity (*P*) is calculated using an effective medium approximation or Lorentz−Lorenz equation, which describes the relation between the optical characteristics and the porosity of the film. Open porosity is calculated from the variation of the refractive index during the absorption and desorption of organic solvents. The relative volume of open and closed pores is calculated by comparing the results obtained with empty and filled pores (before and after adsorption). The pore radius and PRD are calculated from the adsorption and desorption isotherms of the chosen adsorptive (toluene in this particular case). Two different theories are used for the calculation of the pore radius distribution in mesoporous and microporous films. The PRD calculation in the mesoporous films uses the Kelvin equation. For micropores with widths of order of a few molecular diameters, the Kelvin equation is no longer valid. To analyze the microporous films, a method based on a theory developed by Dubinin and Radushkevitch (DR) has been chosen.[19] The EP software recognizes the presence of micropores in the film by analyzing the adsorption/desorption isotherms and calculates both the mesopore and micropore volume and size. A more detailed description of the method can be found elsewhere.[14,19−20]

Depth-profiled PALS was used to determine the micropore and mesopore sizes and pore interconnectivity. Details of the PALS setup and measurement methods appear elsewhere.[21] A monoenergetic positron beam implants positrons into the film with a mean implantation depth controlled by the selected beam energy (1−8 keV). Positronium (Ps), the bound state of a positron and electron, is formed by electron capture and traps in the void volume of pores. The Ps annihilation lifetime (2−142 ns) is correlated with pore size using the extended Tao−Eldrup model.[22] PALS spectra with $\sim 10^7$ events were acquired at room temperature using a conventional fast lifetime system with a time resolution of ~500 ps, and the POSFIT program was used for data fitting.

The refractive index and thickness of the films were measured using a spectroscopic ellipsometer with $\lambda = 350-850$ nm (SENTECH 801) and a prism coupler (Metricon Co., Prism coupler 2010). The dielectric constant was measured at a frequency of 100 kHz using an LCR meter (HP4284)-equipped probe station with MIM (metal−insulator−metal) structure.

The hardness (*H*) and elastic modulus (*E*) of the thin films were measured using the continuous stiffness measurement (CSM) nanoindentation method.[23] In this technique, not only is the force required as a function of indentation depth recorded while a three-sided Berkovich diamond indenter is pushed into the sample and then withdrawn, but also the contact stiffness for all depths are measured by superimposing a small oscillation to the force signal at a relatively high frequency. The amplitude and frequency employed for this experiment were 1 nm and 45 Hz, respectively. Multiple points (typically, six points) on each sample were indented, and the average hardness and elastic modulus are reported to ensure reliability.

TABLE 1: Film Properties of Porous Thin Films Prepared with mCSSQ and Various Content of tCD Compounds

sample	refractive index[a]	thickness[a] (nm)	porosity[b] (%)	% relative porosity[c]	% matrix porosity[d]
mCSSQ	1.4138	1206.1	10	0	10
mCSSQ/tCD 10%	1.3758	1069.2	18	8.2	9.8
mCSSQ/tCD 20%	1.3350	1129.5	26	17.2	8.8
mCSSQ/tCD 30%	1.3183	1014.9	31	21.0	10
mCSSQ/tCD 40%	1.3018	959.0	33	24.7	8.3

[a] Refractive index ($\lambda = 632$ nm) and thickness of the films were measured by spectroellipsometer. [b] Porosity of the films measured by ellipsometric porosimetry. (The volume of adsorbed toluene was normalized to the film volume.) [c] Relative porosity calculated by the Lorentz−Lorentz equation: $P\ (\%) = 1 - [(N_p^2 - 1)/(N_p^2 + 2)]/[(N_m^2 - 1)/(N_m^2 + 2)]$, where N_m is the refractive index of the matrix film (tCD wt % = 0) and N_p is the refractive index of the porous film. The values reflect artificial porosity introduced by porogen. [d] Porosity of the matrix material calculated as the difference between EP porosity[b] and relative porosity[c].

3. Results and Discussion

Table 1 shows the variation of refractive index of the thin films as a function of the porogen content in the precursor coating. The refractive index of the films decreases and porosity increases with increasing porogen concentration, as expected. However, at higher porogen concentration, the change in porosity becomes smaller than the expected value, as shown in Figure 1a. At the same time, Figure 1b shows that the mean pore diameters measured by EP and PALS increases only slightly with increasing porogen concentration. This phenomenon could be explained by pore collapse, as depicted in Figure 2. At the low porogen concentration (<10 wt %), the CD porogen molecules may individually disperse in the matrix precursor and the pore diameter is equal to the diameter of the coiled molecule in the mCSSQ matrix. Therefore, "artificial" or engineered porosity generated from CD decomposition is almost equal to the expected value under low porogen concen-

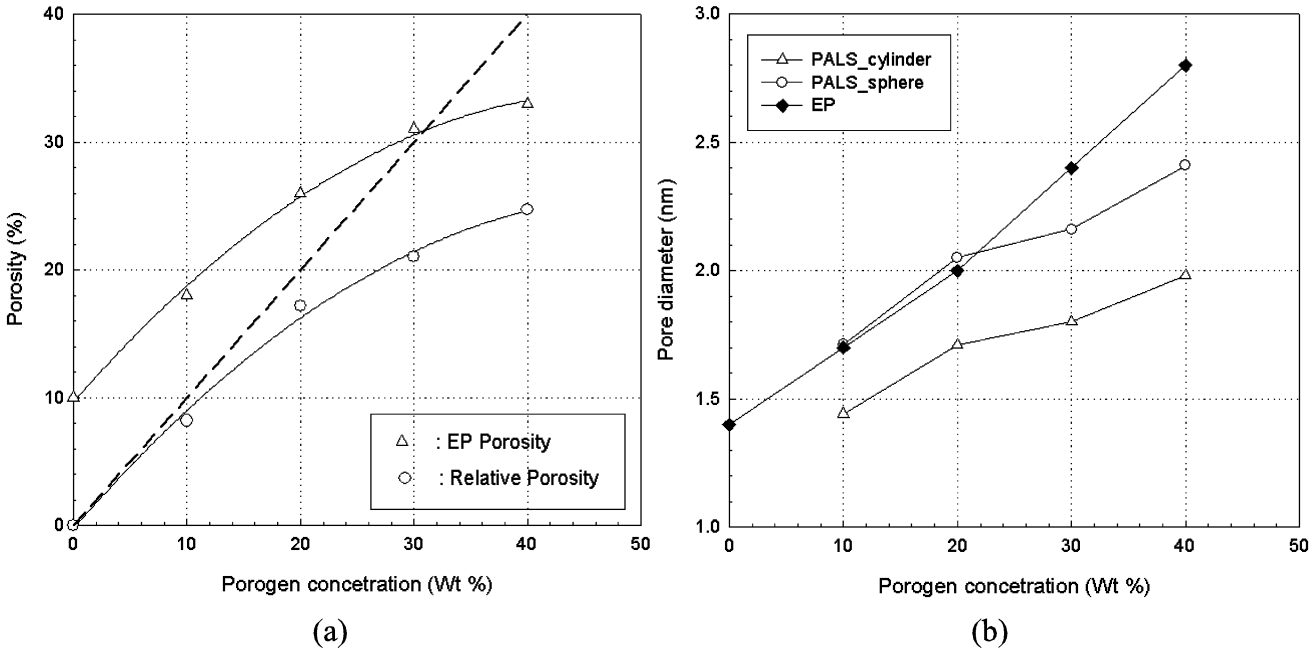

Figure 1. (a) Variation of porosity as a function of CD loading. (b) Pore diameters determined by EP and PALS. It is necessary to mention that EP pore diameter at porogen concentration of 30% and 40% shown in this graph reflect only large pores. Smaller pores determined from deconvolution of PRD curves are closer to the diameters determined by PALS.

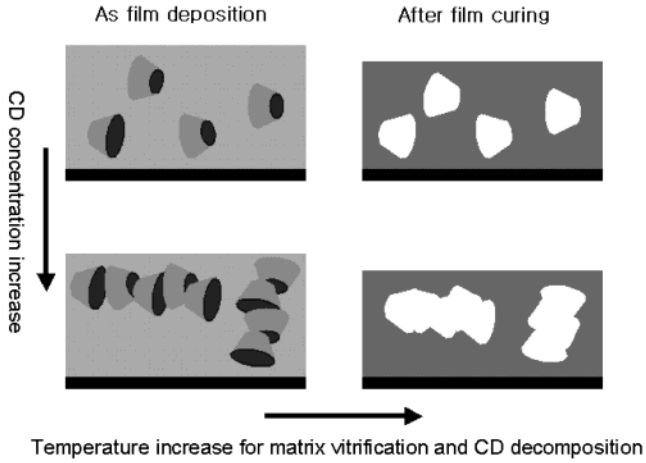

Figure 2. A possible model of agglomeration of CD molecules and pore collapse during the matrix vitrification and CD porogen decomposition.

tration. At the high porogen concentration (>30 wt %), however, CD porogen molecules may interact more favorably. Polarz et al. reported that the pore structure of porous silica materials made from hydrophilic cyclodextrins in aqueous solution as template show a "wormlike" pore system due to a linear interaction of CD molecules.[24] They performed molecular modeling calculations of assemblies of CD molecules and found that it is energetically favorable for the CD complexes to line up in slightly bent or staggered geometries. Therefore, at high CD concentration, CD molecules could linearly interact with each other in the coating precursor (Figure 2). The film should shrink from the condensation reaction of the residual Si−OH group in mCSSQ precursors under the decomposition of CD-based porogen, and eventually pore collapse could occur as depicted in Figure 2. Hence, the pore size could be slightly bigger than the original CD's diameter, and the pore shape may be crudely cylindrical. Figure 3 shows the EP-deduced pore size distribution of various porous mCSSQ thin films as a function of porogen concentration. The average pore radius increases with porogen concentration and the pore radius distribution becomes broader. The films prepared with 10% and 20% porogen concentration have a well-pronounced single peak in the PRD. The PRD in the films prepared with 30% and 40% porogen can be deconvoluted into two peaks with two different sizes. This observation suggests the coexistance of monomeric and agglomerated CD porogen molecules during the preparation of the films with different porogen loading. The degree of agglomeration apparently increases with the porogen concentration. This indicates that CD molecules assemble with each other randomly with increasing concentration, with the result being that various sizes of artificial pores may be generated statistically.

The porous mCSSQ thin films having different CD concentrations were analyzed by depth-profiled PALS. Three positron beam energies were employed, 1.1, 2.1, and 4.1 keV, corresponding to mean positron implantation depths (for a film of density 1.0 g/cm^3) of 30, 90, and 270 nm respectively. The mCSSQ film without porogen does not present any mesoporous Ps signal. It does present a very robust Ps signal annihilating in micropores, as represented by two strong Ps components of 2.9 and 5.9 ns with 18% and 22% relative intensities (i.e. 40% of all incoming positrons annihilate as Ps in the micropores). There is no indication of any Ps escapes through interconnected micropores into the vacuum, so we assume these inherent voids in mCSSQ are isolated (not interconnected) when Ps is used as the pore probe. These two short Ps lifetimes could therefore correspond to spherical pore diameters of 0.71 and 1.03 nm and there may well be a distribution of micropores over this range. The porous mCSSQ thin films prepared with CD-based porogen have an additional Ps lifetime due to the porogen induced "artificial" pores as summarized in Table 2. The pore size deduced using either a spherical or cylindrical pore model also increases with porogen concentration in the spin-coating solution. This trend is consistent with the EP results (See Figure 1b). The pore mean free path (MFP = $4V/S$, where V and S are the pore volume and surface area, respectively) range is set from the two pore models: The MFP in a long cylinder is equal to

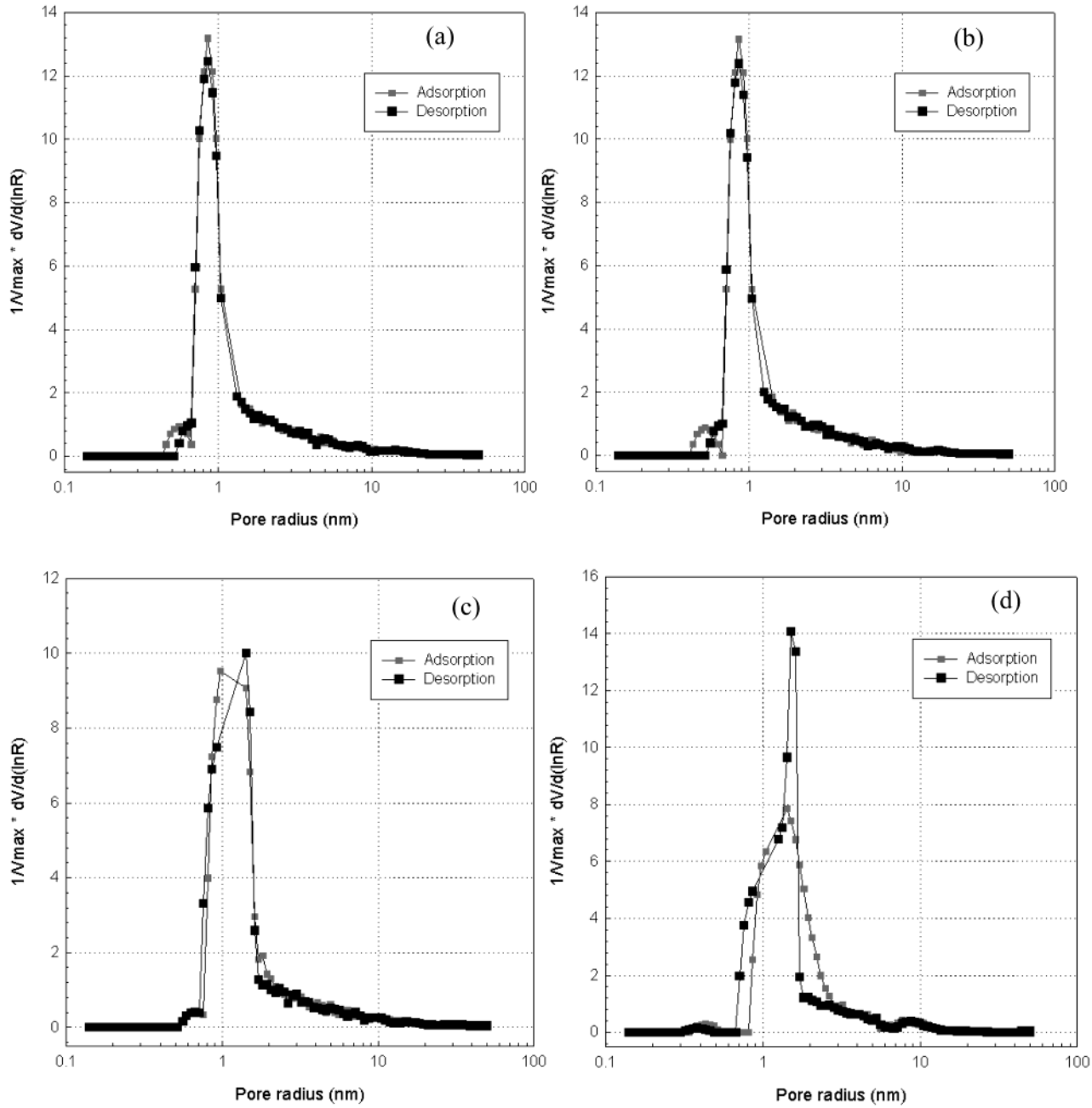

Figure 3. Pore size distributions of porous thin films prepared with mCSSQ and various content of tCD compounds: (a) mCSSQ/tCD 10%, (b) mCSSQ/tCD 20%, (c) mCSSQ/tCD 30%, (d) mCSSQ/tCD 40%.

TABLE 2: Summary of PALS Results for the Mesopores of the mCSSQ Thin Films Prepared with Different Porogen Concentrations

sample	Ps lifetime (ns)	$D_{cylinder}$ (nm)	D_{sphere} (nm)	MF path (nm)	interconnection length (nm)
mCSSQ/tCD 10%	17.0	1.44	1.71	1.14−1.44	<10
mCSSQ/tCD 20%	24.0	1.71	2.05	1.37−1.71	~10
mCSSQ/tCD 30%	26.5	1.80	2.16	1.44−1.80	30
mCSSQ/tCD 40%	31.5	1.98	2.41	1.61−1.98	100

the cross sectional diameter, whereas the MFP in a sphere is $^2/_3$ the sphere diameter. In these films our physical intuition, as discussed in Figure 2, tends to favor the cylindrical pore model and hence the larger value of MFP.

The interconnection length is the effective depth from which Ps can diffuse through the porous network and escape into the vacuum—it is in effect the Ps diffusion length normal to the surface. The prepared porous mCSSQ thin films with varying porogen concentration have some degree of pore interconnectivity—they all have some detectable Ps escaping into the vacuum. It is very small for the 10% film and the pore interconnection length is estimated to be well under 10 nm. However, this film has 3−10% of the Ps formed in the artificial pores escaping into the vacuum and therefore we would not say that this film has rigorously "closed pores". The fraction of Ps escaping into the vacuum for the three different beam implantation energies is plotted in Figure 4a. Typically we extrapolate the first two nonzero points back to zero and if we do that here we consistently get a percolation threshold (or porogen loading corresponding to the closed-to-open pore threshold) of about 5% (Figure 4b). This very low value of the threshold implies that this CD porogen appears to have a tendency to form interconnected pores in the mCSSQ matrix, since virtually all porogen loadings produce some degree of pore interconnectedness.

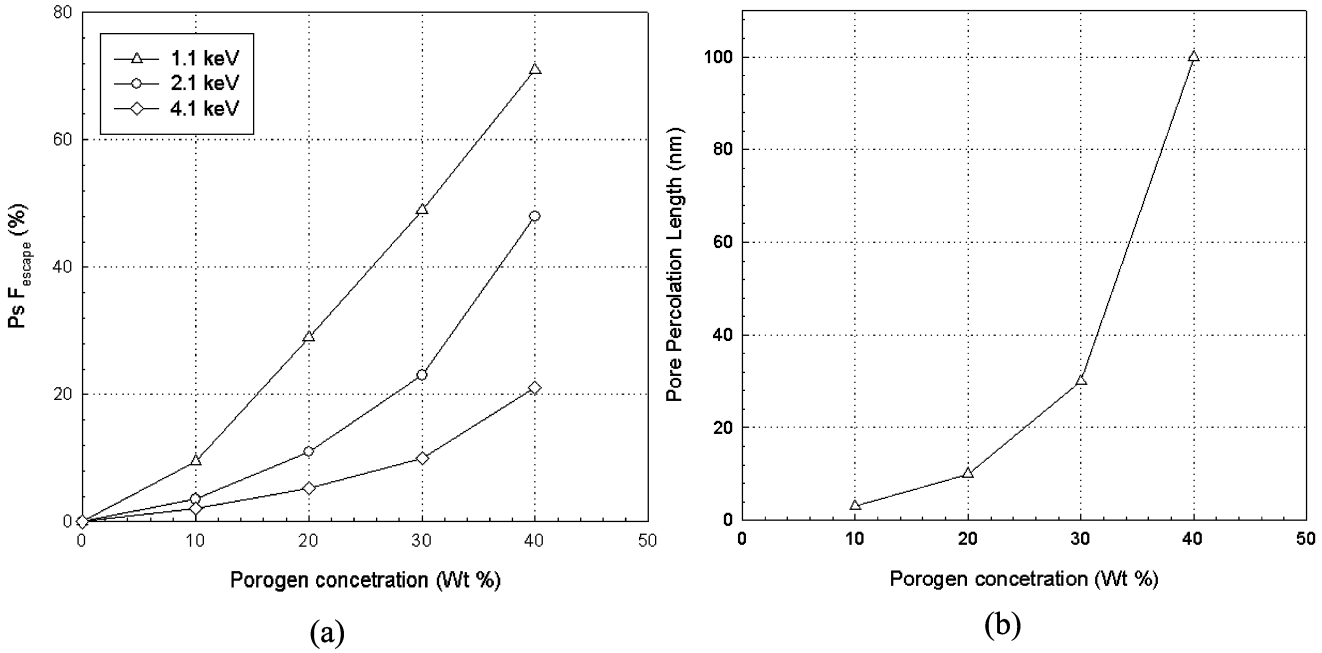

Figure 4. Variation of pore interconnection length as a function of porogen loading. (a) The fraction of Ps escaping into the vacuum for the different positron beam implantation energies. (b) The pore interconnection length deduced by PALS.

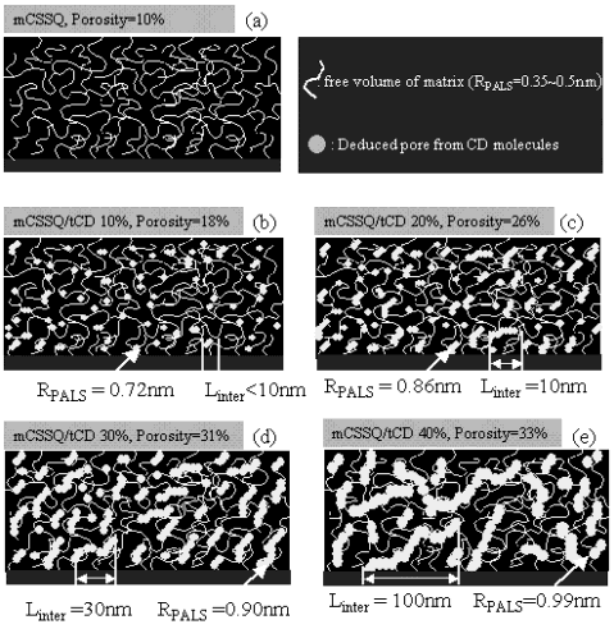

Figure 5. Conceptual drawing of plausible pore structures in the porous thin film from the mCSSQ/tCD system. The porosity was measured by EP. R_{PALS} and L_{inter} denote the average radius and interconnection length measured by PALS, respectively.

From the above investigation of porous mCSSQ thin films by means of two kinds of pore analysis tools, we could generate simple conceptual drawings of porous mCSSQ thin films with different porosities as shown in Figure 5. There are some toluene-accessible micropores in the dense mCSSQ matrix (by means of EP analysis), even if we found that the micropores were isolated from PALS measurement. The measured intrinsic porosity of the matrix is about 10% due to its molecular free volume (see Table 1). This seeming contradiction in the pore interconnectivity determined by PALS and EP is related to different features of Ps and toluene diffusion in micropores with a complicated shape. The diffusion length of the probe species depends on the their chemical properties and lifetime. More

TABLE 3: Electrical and Mechanical Property of Porous Thin Films Prepared with mCSSQ and Various Content of tCD Compounds

		mechanical property		electrical property	
sample	thickness (nm)	hardness (GPa)[a]	modulus (GPa)[a]	dielectric constant (k)[b]	dissipation factor[b]
mCSSQ	1428.8	1.21	6.12	2.64	0.003
mCSSQ/tCD 10%	1467.6	0.90	4.42	2.34	0.002
mCSSQ/tCD 20%	1337.3	0.75	3.68	2.28	0.002
mCSSQ/tCD 30%	1175.4	0.59	3.36	2.13	0.002
mCSSQ/tCD 40%	1173.8	0.53	2.67	1.98	0.001
mCSSQ/tCD 50%	1036.9	0.48	2.50	1.93	0.001

[a] Mechanical properties were measured by nanoindentation, and hardness and elastic modulus of all films were collected at the indentation depth of 100 nm. [b] Measured at 100 kHz.

detailed discussions of this matter will occur in our future publications. Therefore, the pore structure of the dense mCSSQ film may have toluene-accessible intrinsic micropores in the whole film, as shown in Figure 5a. At low porogen concentration, below 10 wt %, most of the artificial pores are randomly distributed as a single molecular dispersion. At increasing porogen concentration, the artificial pores become linearly agglomerated and more pore collapse may occur as a cylindrical pore structure forms (Figure 5b−e). The interconnection length and pore size increase with increasing porogen concentration through porogen agglomeration and/or pore collapse.

To know the relationship between the pore structure and film properties, we monitored dielectric constant, modulus, and hardness of porous mCSSQ thin films having different pore structure, as summarized in Table 3. Figure 6 shows elastic modulus and hardness of various CSSQ-based thin films as a function of displacement. We made thick films above 1000 nm in order to eliminate the substrate effect in nanoindentation. Values of hardness and modulus of all films were collected at an indentation depth of 100 nm. Mechanical properties of the films linearly decrease with increasing porosity (Figure 7a) in the evaluated range of porosity from 10 to 40%. The change of the dielectric constant with density/porosity is well-described by the Clausius−Mossotti equation, which suggests that the

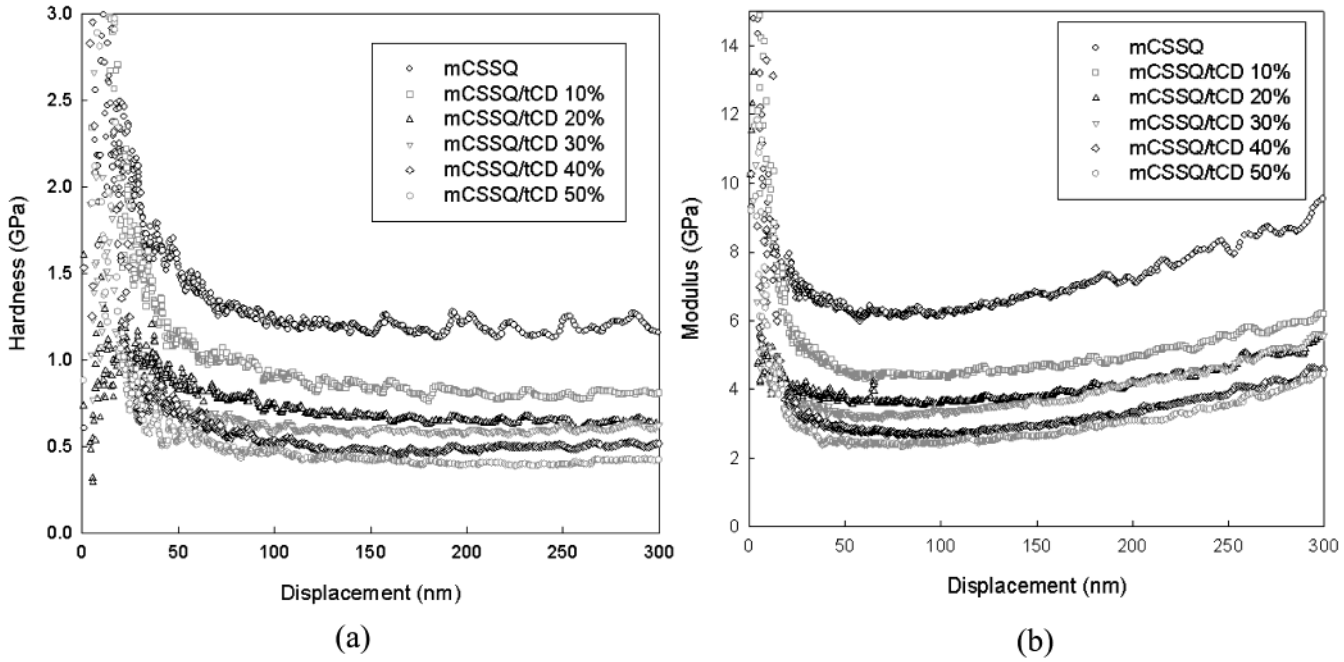

Figure 6. (a) Hardness and (b) elastic modulus values, plotted as function of indentation depth of porous mCSSQ thin films.

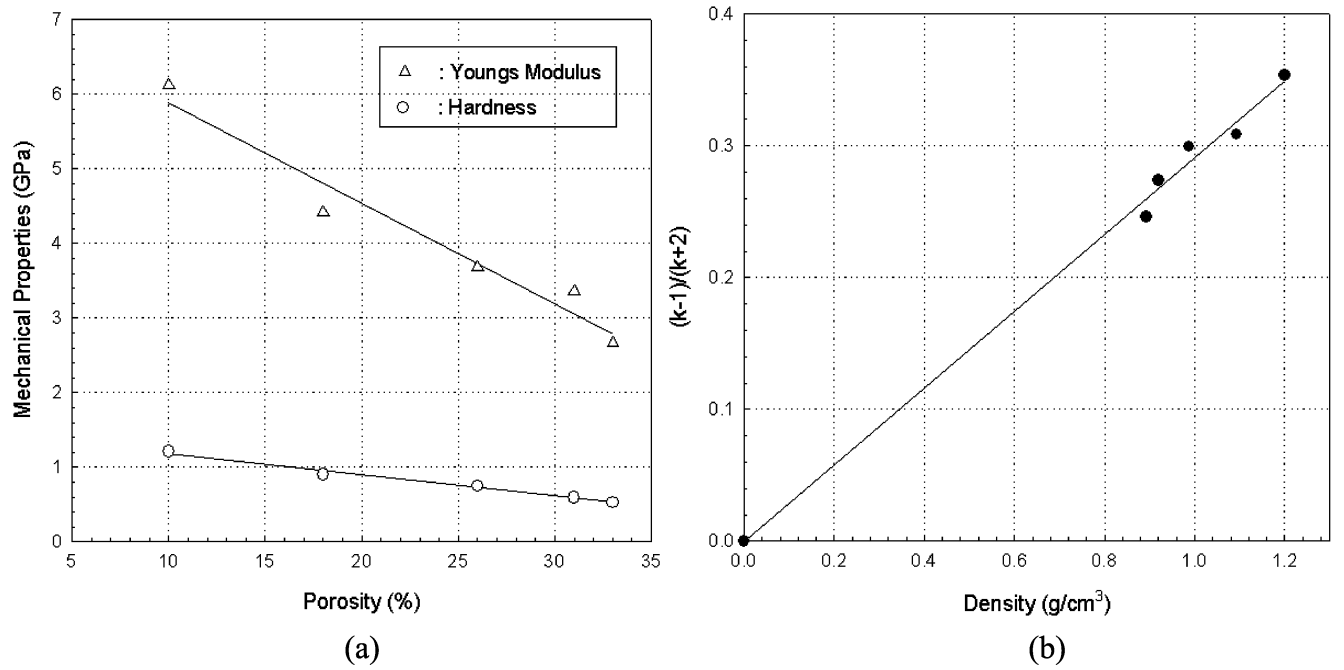

Figure 7. (a) Variation of mechanical property and (b) variation of polarizability of porous mCSSQ thin films.

molecular polarizability of the matrix material does not change with introduction of porosity (Figure 7b).

4. Conclusions

The pore structure of porous mCSSQ thin films were investigated as a function of porogen concentration by means of both EP and PALS. Under low porogen concentration (<10 wt %), most nanopores appear to be isolated and dispersed, while porogen agglomeration and pore collapse become severe with increasing porogen concentration. Moreover, porosity increases and pore size distribution increases and broadens with increasing porogen concentration due to CD porogen agglomeration subsequent pore collapse in the mCSSQ matrix. The pore interconnection threshold of the mCSSQ/tCD film system was small (about 5% as determined by PALS) and the interconnected pore shape could be postulated as a cylinder-like structure, owing to the tendency of CD molecules to linearly attract. The dielectric constant and mechanical properties of the porous mCSSQ thin film decreased with increasing porosity, as reported elsewhere.

References and Notes

(1) Kresge, C. T.; Leonowicz, M. E.; Roth, W. J.; Vartuli, J. C.; Beck, J. S. *Nature* **1992**, *359*, 710.

(2) Asefa, T.; MacLachlan, M. J.; Coombs, N.; Ozin, G. A. *Nature* **1999**, *402*, 867.

(3) Corma, A. *Chem. Rev.* **1997**, *97*, 2373.

(4) Zhao, D.; Feng, J.; Huo, Q.; Melosh, N.; Fredrickson, G.; Chnelka, B.; Stucky, G. *Science* **1998**, *279*, 548.
(5) Zhao, D.; Sun, J.; Li, Q.; Stucky, G. *Chem. Mater.* **2000**, *25*, 275.
(6) Kim, H. C.; Wilds, J. B.; Kreller, C. R.; Volksen, W.; Brock, P. J.; Lee, V. Y.; Magbitang, T.; Hedrick, J. L.; Hawker, C. J.; Miller, R. D. *Adv. Mater.* **2002**, *14*, 22, 1637.
(7) Hedrick, J. L.; Miller, R. D.; Hawker, C. J.; Carter, K. R.; Volksen, W.; Yoon, D. Y.; Trollsas, M. *Adv. Mater*. **1998**, *10*, 1049.
(8) Nguyen, C. V.; Carter, K. R.; Hawker, C. J.; Hedrick, J. L.; Jaffe, R. L.; Miller, R. D.; Remenar, J. F.; Rhee, H. W.; Rice, P. M.; Toney, M. F.; Trollsas, M.; Yoon, D. Y. *Chem. Mater.* **1999**, *11*, 3080.
(9) Kohl, A. T.; Mimna, R.; Shick, R.; Rhodes, L.; Wang, Z. L.; Kohl, P. A. *Electrochem. Solid-State Lett.* **1999**, *2* (2), 77.
(10) deTheije, F. J.; Balkenendl, A. R.; Verheijen, M. A.; Baklanov, M. R.; Mogilnikov, K. P.; Furukawa, Y. *J. Phys. Chem.* **2003**, *107*, 4280.
(11) Yang, S.; Mirau, P. A.; Pai, C.; Nalamasu, O.; Reichmanis, E.; Pai, J. C.; Obeng, Y. S.; Seputro, J.; Lin, E. K.; Lee, H.; Sun, J.; Gidley, D. W. *Chem. Mater.* **2002**, *14*, 369.
(12) Yim, J.-H; Lyu, Y.-Y.; Jeong, H.-D.; Song, S. A.; Hwang, I.-S.; Hyeon-Lee, J.; Mah, S. K.; Chang, S.; Park, J.-G.; Hu, Y. F.; Sun, J. N.; Gidley, D. W. *Adv. Funct. Mater.* **2003**, *13* (5), 386.
(13) Rouquerol, J.; Anvir, D.; Fairbridge, C. W.; Everett, D. H.; Haynes, J. H.; Pernicone, N.; Ramsay, J. D. F.; Sing, K. S. W.; Unger, K. K. *Pure Appl. Chem*. **1994**, *66*, 1739.
(14) Baklanov, M. R.; Mogilnikov, K. P.; Polovinkin, V. G.; Dultsev, F. N. *J. Vac. Sci. Technol. B* **2000**, *18*, 1385.
(15) Gidley, D. W.; Frieze, W. E.; Dull, T. L.; Sun, J.; Yee, A. F.; Nguyen, C. V.; Yoon, D. Y. *Appl. Phys. Lett*. **2000**, *76* (10), 1282.
(16) Wu, W.-I.; Wallace, W. E.; Lin, E. K.; Lynn, G. W.; Glinka, C. J.; Ryan, E. T.; Ho, H. M. *J. Appl. Phys.* **2000**, *87*, 1193.
(17) Huang, E.; Toney, M. F.; Volksen, W.; Mecerreyes, D.; Block, P.; Kim, H.-C.; Hawker, C. J.; Hedrick, J. L.; Lee, V. Y.; Magbitang, T.; Miller, R. D. *Appl. Phys. Lett.* **2002**, *81*, 2232.
(18) Yim, J.-H.; Lyu, Y.-Y.; Jeong, H.-D.; Mah, S. K.; Hyeon-Lee, J.; Hahn, J.-H.; Kim, G. S.; Chang., S.; Park, J.-G. *J. Appl. Polym. Sci.* **2003**, *90*, 626.
(19) Baklanov, M. R.; Mogilnikov, K. P. *Microelectronic Eng.* **2002**, *64*, 1−4, 335.
(20) Maex, K.; Baklanov, M. R.; Shamiryan, D.; Iacopi, F.; Brongersma, S.; Yanovitskaya, Z. Sh. *J. Appl. Phys.* **2003**, *93*, 11, 8793.
(21) Gidley, D. W.; Frieze, W. E.; Yee, A. F.; Dull, T. L.; Ho, H.-M.; Ryan, E. T. *Phys. Rev. B, Rapid Commun.* **1999**, *60* (8), R5157.
(22) Dull, T. L.; Frieze, W. E.; Gidley, D. W.; Sun, J. N.; Yee, A. F. *J. Phys. Chem. B.* **2001**, *105* (20), 4657.
(23) Oliver, W. C.; Pharr, G. M. *J. Mater. Res*. **1992**, *7*, 1564.
(24) Polarz, S.; Smarsly, B.; Bronstein, L.; Antonietti, M. *Angew. Chem.* **2001**, *113* (23), 4549.